Research

Excitatory postsynaptic calcium transients at *Aplysia* sensory–motor neuron synapses allow for quantal examination of synaptic strength over multiple days in culture

Tyler W. Dunn and Wayne S. Sossin

Department of Neurology and Neurosurgery, Montreal Neurological Institute, McGill University, Montreal, Quebec H3A 2B4, Canada

A more thorough description of the changes in synaptic strength underlying synaptic plasticity may be achieved with quantal resolution measurements at individual synaptic sites. Here, we demonstrate that by using a membrane targeted genetic calcium sensor, we can measure quantal synaptic events at the individual synaptic sites of *Aplysia* sensory neuron to motor neuron synaptic connections. These results show that synaptic strength is not evenly distributed between all contacts in these cultures, but dominated by multiquantal sites of synaptic contact, likely clusters of individual synaptic sites. Surprisingly, most synaptic contacts were not found opposite presynaptic varicosities, but instead at areas of pre- and postsynaptic contact with no visible thickening of membranes. The release probability, quantal size, and quantal content can be measured over days at individual synaptic contacts using this technique. Homosynaptic depression was accompanied by a reduction in release site probability, with no evidence of individual synaptic site silencing over the course of depression. This technique shows promise in being able to address outstanding questions in this system, including determining the synaptic changes that maintain long-term alterations in synaptic strength that underlie memory.

How changes in neuronal systems underlie memory remains an important outstanding question in neuroscience. Although much research has focused on changes that occur immediately after the stimulus, such as long-term potentiation, it is clear that what is often termed "consolidation," or what perhaps is more correctly termed long-term memory formation, is not simply due to solidifying short-term changes (Sossin 2008). One attractive model for neuronal changes underlying long-term memory formation is the formation of new synapses (Bailey et al. 2015). Whereas there are many correlative studies suggesting increased numbers of synapses after learning, there are few systems where one can examine the number of synapses between identified neurons before or after a stimulus that generates long-term synaptic changes. This is important, because even with new technologies that have been able to document increased numbers of synapses between ensembles of neurons allocated to a memory compared with neurons not allocated to a memory (Choi et al. 2018), it is not clear whether the increased numbers of synapses were present before allocation and helped bias the allocation decision (Kim and Cho 2020) or whether synapse formation and stabilization occurred because of the stimulus. The ideal experiment would be to follow the connections before learning, document the increased number of synapses, and then determine whether the increased number of synapses was important for the increase in synaptic strength between these neurons thought to be important for memory maintenance.

The sensory neuron to motor neuron synapse of *Aplysia* is an important model system that is well suited for this task. In this system one can monitor learning-related long-term changes in synaptic strength in a reduced preparation starting before the stimulation and lasting >1 wk after stimulation (Kandel 2001; Hu et al. 2017a). One of the striking observations in this preparation is that similar to the animal, long-term changes in synaptic strength are accompanied by morphological changes, particularly an increase in presynaptic varicosities (Bailey and Chen 1988; Glanzman et al. 1990; Casadio et al. 1999; Bailey et al. 2015). These studies provide some of the strongest evidence that long-term increases in synaptic strength are supported by an increase in the number of synapses. In this system, blocking reconsolidation or using pharmacological or dominant negative inhibitors of persistent protein kinases erase both sensitization and reduce long-term increases in synaptic strength back to baseline (Cai et al. 2011; Lee et al. 2012; Hu and Schacher 2015; Hu et al. 2017b). Surprisingly, although erasure was associated with a decrease in the number of varicosities, the new varicosities formed after learning were not specifically removed (Chen et al. 2014).

One issue with all of these findings is that synapses in this study were measured by presynaptic varicosities, but these are only a surrogate for actual synaptic sites, except when electron microscopy is used to measure active zones. In the animal, only ~40% of sensory neuron presynaptic varicosities have active zones (Bailey and Chen 1983), and in cultures only ~30% of presynaptic varicosities actively release transmitter based on studies using Synapto-pHluorin (Kim et al. 2003). Moreover, whereas increases in varicosity numbers are usually highly correlated with increases in synaptic strength, there are exceptions. One day of training leads to sensitization without increases in varicosities

Corresponding author: wayne.sossin@mcgill.ca
Article is online at http://www.learnmem.org/cgi/doi/10.1101/lm.052639.120.

(Wainwright et al. 2002); similarly, if application of serotonin is restricted to the cell soma, 24-h increases in synaptic strength are observed in the absence of an increase in varicosities (Sun and Schacher 1998). In summary, because many studies examining mechanisms underlying long-term changes use sensory neuron to motor neuron cultures, it would be beneficial to have a method to identify the individual functional synaptic sites in this system, instead of the surrogate measure of presynaptic varicosities.

In addition to answering questions concerning long-term synaptic changes, the ability to identify individual synaptic sites will also allow a more sophisticated analysis of other plasticity mechanisms, as individual release site probability can be specifically measured rather than relying on averages that cannot separate changes in probability from changes in the number of sites participating. For example, homosynaptic depression of sensory neuron to motor neuron synapses is the cellular basis for behavioral habituation. It has been proposed that this depression is due to the silencing of a subset of synaptic sites, whereas other sites escape synaptic depression and participate in the response that is retained after depression (Royer et al. 2000; Gover et al. 2002; Gover and Abrams 2009). Quantal resolution would be required to address this question by measuring the participation of individual synapses at a synaptic connection during the process of plasticity, and, as such, direct demonstration of synaptic site silencing has not yet been observed.

In vertebrates, many AMPA receptors are impermeable to calcium because of RNA editing of a critical glutamine in the AMPA receptor pore. However, in *Aplysia* there is no evidence for this editing in any AMPA receptor cDNA sequence (Greer et al. 2017), and invertebrate AMPA receptors without this modification are calcium permeable (Li et al. 2016). Thus, one can image synaptic transmission in *Aplysia* using calcium-sensitive dyes that detect calcium transients in the postsynaptic cell that are locked to the action potential, and these excitatory postsynaptic calcium transients (EPSCaTs) are blocked by AMPA receptor antagonists (Malkinson and Spira 2010).

Using this technique ~56% of presynaptic varicosities adjoined postsynaptic calcium transients, but only 60% of synapses were at varicosities (Malkinson and Spira 2010). However, this study focused only on regions rich in varicosities and may have underestimated the number of synapses not at varicosities. Instead of calcium dyes used in this previous study, the use of sensitive genetically encoded calcium sensors that are membrane delimited can be used to detect synapse location in invertebrates (Akbergenova et al. 2018). Here, we present data using expression of a calcium sensor to localize synapses in neuronal cultures with *Aplysia* sensory neurons and motor neuron. Using strict criteria to define EPSCaTs we find that most EPSCaTs are not found at varicosities. EPScaTs were stable over days, and this technique shows promise in being able to address the question of whether new synapses account for the increases in synaptic strength thought to be important for memory maintenance.

An initial attempt to address whether homosynaptic depression is due to individual synaptic site silencing using EPSCaTs suggested depression occurred through reduction in release probability; however, without demonstrating quantal resolution, changes in the number of participating sites cannot be differentiated from changes in release probability (Malkinson and Spira 2013). With the improved localization of the calcium transient using a membrane-delimited calcium sensor, quantal resolution was possible. Many of the EPSCaTs are made up of multiple quanta, likely indicating that these sites are in tight clusters. Thus, without the quantal resolution described here, any synaptic imaging in this system could be biased toward these clustered synaptic release sites where it is particularly difficult to differentiate changes in the number of participating sites versus changes in release probability. Through examining the isolated, putative uniquantal sites of release, we find no evidence for individual synaptic site silencing during cellular depression; instead homosynaptic depression follows a reduction in transmitter release probability.

Results

Generation of a calcium sensor optimized for visualizing synaptic calcium transients

To address important issues of synapse specificity and whether new synaptic sites formed by learning participate in the increases in synaptic strength (Sossin 2018) requires a technique that can both localize synaptic sites over days in culture and measure the strength of individual synaptic sites. Pioneering work using calcium indicator dyes showed that EPSCaTs, mediated mainly by calcium flowing through calcium-permeable AMPA receptors, can be used to localize and measure the strength at synaptic sites in *Aplysia* sensory–motor neuron cultures (Malkinson and Spira 2010; Malkinson and Spira 2013). However, calcium dyes tend to compartmentalize over time (Paredes et al. 2008), making multiday use problematic. Moreover, their mobile cytoplasmic location results in substantial diffusion of the fluorescent calcium signal from its site of entry, limiting the fine resolution of synapse location. Genetically encoded calcium sensors, such as GCaMP (Nakai et al. 2001), can solve these issues. Adding protein determinants that limit the GCaMP to membranes can decrease the spread of the synaptic calcium fluorescence signal. Calcium entering across the plasma membrane would most likely interact with the membrane-delimited GCaMP subpopulation at the site of entry, the synapse, and have minimal diffusion while fluorescent as the calcium-bound GCaMP is membrane bound (Shigetomi et al. 2010). We limited GCaMP6s to membranes by fusing it to the *Aplysia* Src amino terminal that contains myristylation and palmitylation signals (src-GCamP6s), similar to previous membrane-delimited versions of GCaMP (Shigetomi et al. 2010; Akbergenova et al. 2018). We believe this approach is better than using a transmembrane domain because of the lack of a requirement for passage through the secretory system, often leading to accumulation in the endoplasmic reticulum (ER), as we have observed for other tagged transmembrane proteins expressed in *Aplysia* sensory neurons (Nagakura et al. 2008; Farah et al. 2019).

Src-GCAMP6s is effective at measuring action potential–evoked calcium transients

Single *Aplysia* sensory neurons were cultured with single LFS motor neurons for 3 d, and synaptic connections formed that were composed of multiple synaptic release sites. On the third day, nuclear injection of plasmids containing RFP into the presynaptic sensory neuron and src-GCaMP6s into the postsynaptic motor neuron was carried out, and the cultures left a further day to allow for plasmid expression (Fig. 1A). Intracellular sharp electrodes were used to control and measure membrane potential of both the presynaptic and postsynaptic neurons. Image acquisition (25-msec exposure, ~17 Hz) was synchronized to the stimulus pulse to standardize data acquisition of evoked synaptic transmission and allow for automatic processing of the large data set associated with each experiment. We acquired nine images to serve as a baseline fluorescence signal, evoked a presynaptic action potential during frame 10, and continued imaging for 35 more frames. Subtraction of the frame preceding the action potential (frame 9) from the frame immediately following the action potential (frame 11) produces an image of the calcium transient occurring during the given stimulus (Fig. 1B).

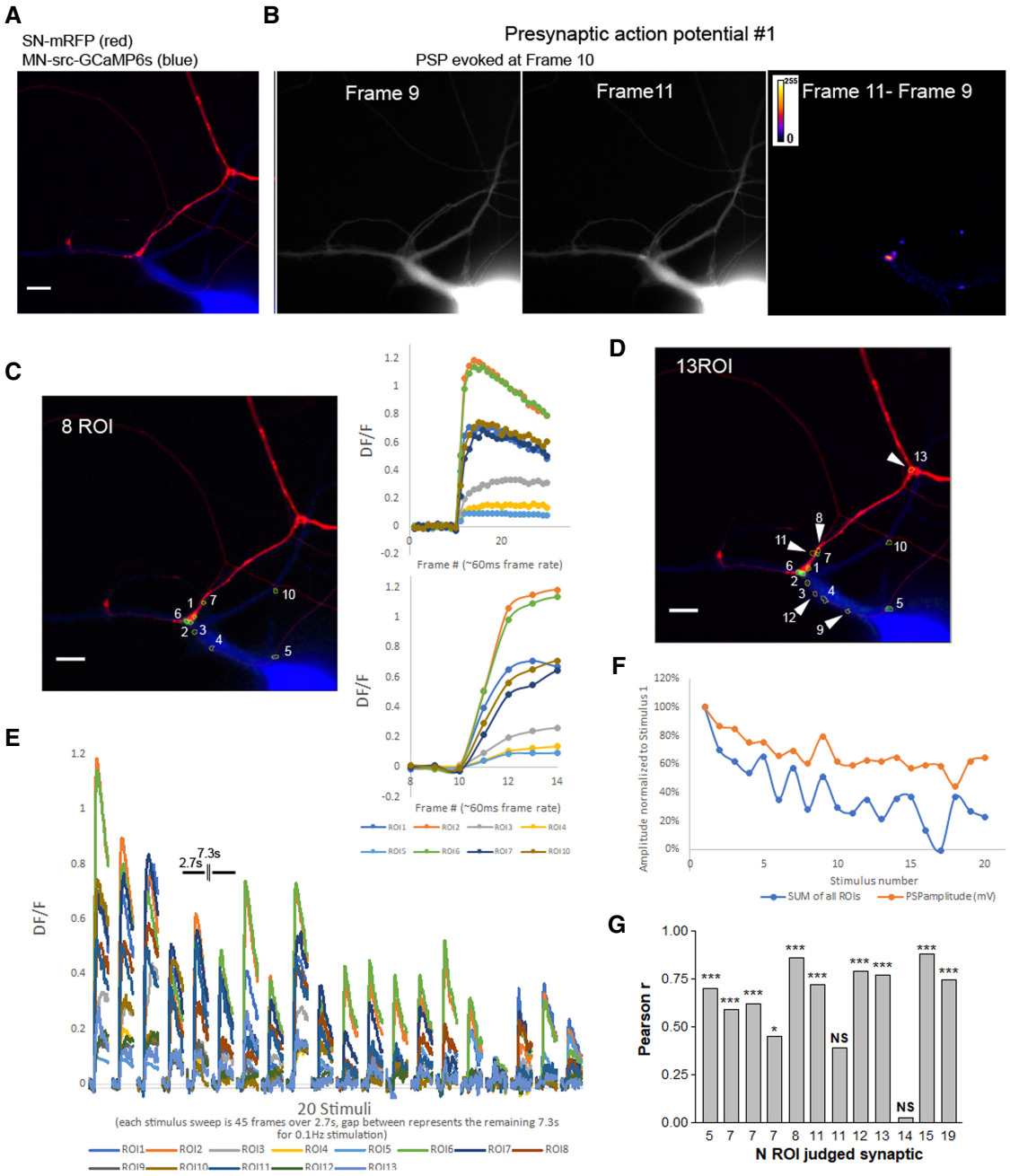

Figure 1. Evoked synaptic transmission at the *Aplysia* sensory to motor neuron synapses measured with postsynaptic src-GCaMP6s calcium transients. (*A*) Image of the synaptic pair, with the presynpatic neuron expressing RFP (red) and the postsynaptic neuron expressing src-GCaMP6s (blue). (*B*) With 45 frames taken, an action potential is evoked during the 10th frame. Subtracting the src-GCaMP6s fluorescence intensity measured from frame 9 (taken immediately preceding the action potential) from the src-GCaMP6s signal from frame 11 (taken immediately following the action potential) reveals the src-GCaMP6s transient in the resulting image produced (*right* panel; intensity presented in a "fire" look-up table with the calibration bar for the calculation results of the image subtraction in arbitrary units). Scale bar, 20 µm. (*C*) Using the same image as in *A* for the presynaptic RFP and postsynaptic src-GCaMP6s (blue), the frame 11 – 9 image subtraction image for a single stimulus (Stimulus #1) is in the green channel and is used to find regions of interest (ROIs) that are labeled. Intensity at each ROI is normalized into a *DF*/*F* using the average of frame 1–9 as F_0. (*Top right*) The transients can be seen to have variable amplitude and various time courses. (*Bottom right*) The rise rate of the transients can be seen more clearly just focusing on frames 9–14. (*D*) To gather additional data about the synaptic connections examined, 20 stimuli are delivered at 0.1 Hz. Red and blue channels are as in *A*, however the green channel is now the summation of the frame 11 – frame 9 images for all 20 stimuli. Because not all synapses participate in the first stimulus, additional ROIs are identified (five new ROIs shown by arrows in the example shown). (*E*) The transients at each of the ROIs shown in *C* are overlayed to show the variation in amplitude between ROIs and from stimulus to stimulus. (*F*) Postsynaptic potential (PSP) amplitude undergoes characteristic homosynaptic depression with these 20 successive presynaptic action potentials, as does the intensity of the summed *DF*/*F* values measured at all the ROIs with strong correlation between the PSP amplitude and the summed *DF*/*F* values (Pearson's r 0.8265, $P < 0.000001$). (*G*) Bar graph of the Pearson's r values for the correlation between PSP amplitude and the sum of the frame 11 *DF*/*F* values from synaptic connections examined with five or more ROIs within the field of view (the number of ROIs in each trial is used as the *x*-axis label). Only synapses with a Pearson's r value that produces a *P*-value of $P < 0.05$ will be further examined; therefore, trials with <5 ROI or a $P > 0.05$ would not be used in analysis. (**) $P < 0.01$, (***) $P < 0.001$. The two trials removed for having a non-significant correlation between PSP amplitude and the evoked src-GCaMP6s transient amplitude are shown.

To identify and analyze synaptic transmission using the postsynaptic calcium transient, regions of interest (ROIs) were selected as described in the Materials and Methods. Multiple ROIs with varying magnitudes of fluorescent changes are observed dispersed throughout the field of view after a single stimulus (Fig. 1C). The peak of the transients tends to occur much later than frame 11; however, as frame 12 is acquired 80–110 msec following the peak of the postsynaptic potential (PSP), and therefore the end of the synaptic current, the source of the calcium leading to the further increases in *DF*/*F* beyond frame 11 are likely from sources other than entry through synaptic glutamate receptors, such as L-type calcium channels (Malkinson and Spira 2010) and neighboring synaptic sites, and thus only data from frame 11 is used for measurements of synaptic strength. To maximize the descriptive data from every sensory to motor neuron pair examined, 20 stimuli were evoked per trial at 0.1 Hz. Summation of all 20 calcium transient images (frame 11 – frame 9 for each stimulus) better describes the entire synapse within a field of view, often revealing sites that did not participate in the first stimulus (Fig. 1D). The number of new ROIs identified with subsequent stimuli reduce so that only 2.0% ± 1.0% ($n = 10$ synaptic connections) of the ROIs first participate in one of the last five stimuli, suggesting that few additional sites would be found with more stimuli. However, if there are very low probability synapses (probability of release near or less than 0.05), these synapses will be undercounted. Moreover, as described below, using 20 stimuli allows for better resolution of the individual ROIs and a far greater data set for more accurate analysis of the quantal nature of the EPSCaTs. Following generation of the full ROI set for a particular synaptic pair, fluorescence intensity is measured for all ROIs over the 20 evoked synaptic stimuli, converting fluorescence intensity into *DF*/*F* values (Fig. 1E). The transients at each ROI over the 20-stimulus trial are independent and variable in amplitude, consistent with transmitter release from independent synapses synchronized by the presynaptic action potential (Fig. 1E). Comparison of the normalized PSP amplitude to the normalized EPSCaT amplitude for each of the 20 stimuli for the synaptic connection described in Figure 1, A–E, shows a strong correlation between these two measurements (Fig. 1F). Examining this over the full data set finds that most trials with five or more ROIs in the field of view show a strong correlation between these two independent measures of synaptic transmission (Fig. 1G). However, in some circumstances, either because of strong and widespread bursts of nonsynaptic calcium transients or to a high proportion of the synapses being outside the field of view, this correlation was not significant and these trials were not used in the analysis (Fig. 1G)

To maximize the chance of seeing all synapses within the field of view, we increased the extracellular calcium to magnesium ratio (55 mM $CaCl_2$, 11 mM $MgCl_2$ as opposed to 11 mM $CaCl_2$, 55 mM $MgCl_2$ in standard saline used for recordings). This is identical to the change in extracellular calcium previously used for measuring EPSCaTs with calcium indicator dyes (Malkinson and Spira 2010; Malkinson and Spira 2013). To determine the extent to which this affected synaptic transmission, we measured the effect of this high calcium recording saline on the amplitude of the PSP. Because the *Aplysia* sensory to motor neuron synapses undergo homosynaptic depression, we measured the change in PSP amplitude going from both normal to high calcium saline and from high to normal calcium saline. Half of the difference in the change in PSP amplitude between these two conditions is equal to the change in PSP amplitude with high calcium saline and was found to be an ~15% increase in PSP amplitude with the high calcium saline (Fig. 2).

Developing criteria for separating EPSCaTs from other calcium transients

Src-GCaMP6s transients can occur frequently in the postsynaptic neuron without any correlation to synaptic membrane potential changes either evoked or spontaneous. These transients have variable time courses and can appear similar to the synaptic transients (Fig. 3A). Although the size of the ROI tends to be much larger with the nonsynaptic transients than those of the synaptic ROIs, the time course of some of these events can appear similar to the synaptic events. In some instances, these transients occur at or near enough to selected ROIs to create coincidental false positive transients during the action potential stimulus. To reduce the impact of these transients that are not directly involved in synaptic transmission, we added an additional criteria at each ROI for inclusion of each transient in subsequent analysis. If a transient initiates prior to frame 10, when the presynaptic action potential occurs, the transient is considered a calcium transient unrelated to direct synaptic transmission. As the nonsynaptic calcium transients have variable rates of occurrence within and from trial to trial, the level of interference in measuring synaptic transmission also varies. The number of events that initiate prior to the stimulus at a chosen ROI

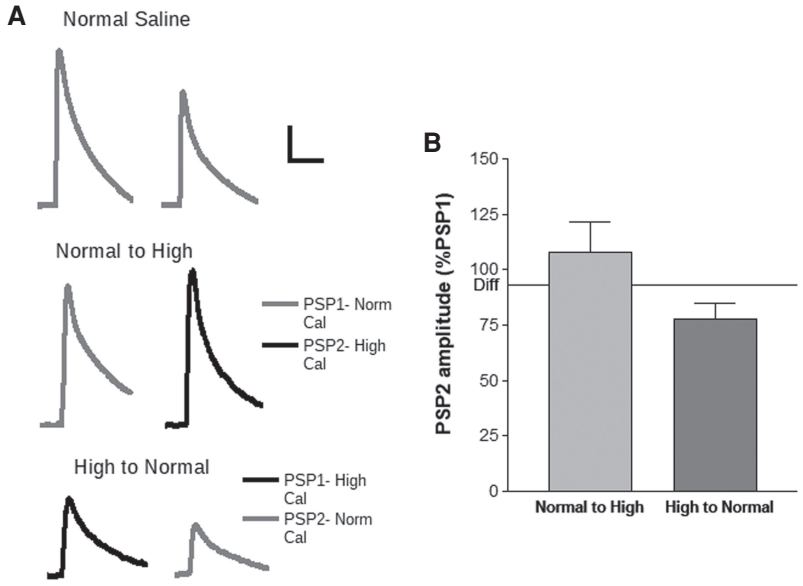

Figure 2. Effects of high calcium saline on PSP amplitude. (*A*) Representative PSP traces. (*Top* traces) PSP1 and PSP2 in normal saline (highlighting synaptic depression). (*Middle* traces) With PSP1 in normal saline (55 mM $MgCl_2$, 11 mg $CaCl_2$), PSP2 evoked following 30 mL perfusion with high calcium saline (11 mM $MgCl_2$, 44 mM $CaCl_2$). (*Bottom* traces) With PSP1 in high calcium saline and PSP2 evoked after perfusion of 30 mL of normal saline. The time between PSPs for saline perfusion was 3–4 min. Scale bars,10 mV/50 msec. (*B*) Summary of the average PSP amplitude change going from normal to high calcium saline ($n = 6$ synaptic connections) and from high calcium to normal calcium saline ($n = 7$ synaptic connections). Error bars are SEM. Because all experiments will undergo synaptic depression and this high calcium buffer does not affect the amount of depression (Malkinson and Spira 2013), the effect of high calcium can be simply calculated by the average of both amplitude changes. This is marked with a bar and is equal to a change in PSP amplitude with high calcium saline at ~15%.

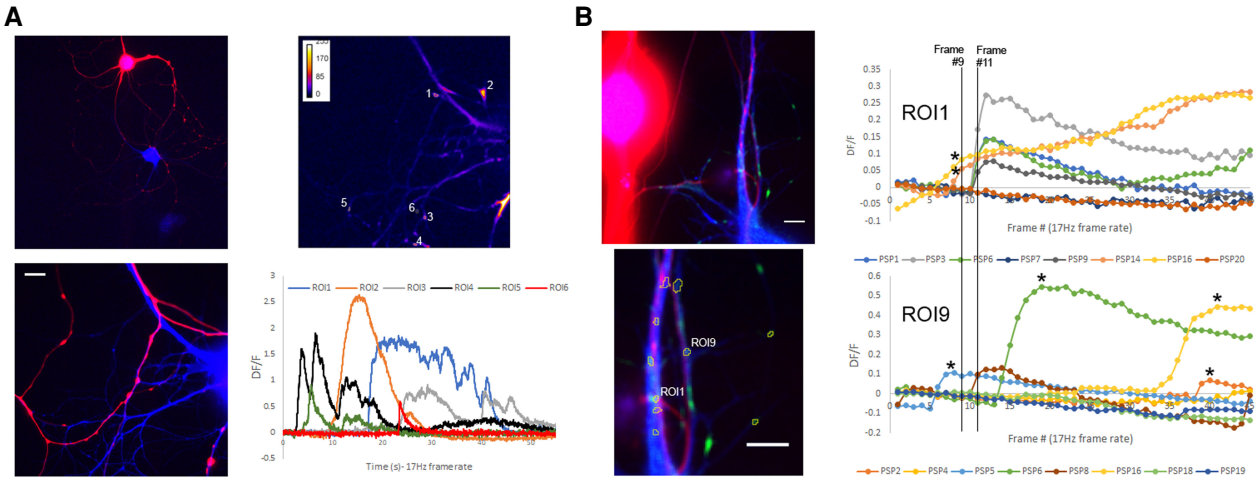

Figure 3. Nonsynaptic calcium transients. (*A*) Representative image of sensory neuron expressing RFP and the postsynaptic neuron expressing src-GCaMP6s, 10× image *above* 40× image. Scale bar, 20 µm. The *top right* panel is a compressed image of the maximum pixel value over a 900-frame acquisition period with the first frame subtracted to remove the baseline fluorescence, with intensity presented in a fire look-up table, highlighting the location and variable size of the nonsynaptic calcium transients (presynaptic neuron was kept quiescent with hyperpolarization and the postsynaptic neuron monitored for any spontaneous mini synaptic transmission during the imaging period). The fluorescence intensity of the ROIs selected in this image are graphed *below* showing the variable time courses of these nonsynaptic calcium transients, using the first nine frames to measure F_0 for each ROI. (*B*) A single trial demonstrating the potential for nonsynaptic events to appear synaptic. Two synaptic ROIs from the synaptic pair shown at the *left* (magnified in the *bottom* image) chosen for the high number of nonsynaptic events occurring during the action potential–evoked synaptic transmission measurements marked with an asterisk. Only some of the 20 PSP sweeps are shown to highlight the synaptic transients (that initiate at frame 11) and the events not directly measuring the synaptic current either through early or late initiation (*). Scale bars, 20 µm.

range from 0 up to a rate of 4.3%, averaging 0.9% ± 0.2% (data from 18 synaptic connections). From this we can estimate that a similar percentage of nonsynaptic calcium transients is also occurring at synaptic ROI during the period when synaptic transients are measured (i.e., a nonsynaptic transient that initiates in frame 10 or frame 11), producing false positives that slip through this filter. Examples of nonsynaptic transients that interfere with EPSCaT measurement are shown in Figure 3B and removed from subsequent analysis. Both trials that were removed for having a nonsignificant correlation between PSP and EPSCaT amplitude (Fig. 1G) had a high number of these transients (3.6% and 4.3%, respectively).

Dissociation of independent ROIs within a cluster with repeated stimuli

Examination of the individual synaptic ROIs reveals a homogeneous area distribution and apparent quantal fluctuations in the action potential–evoked calcium transients measured with src-GCaMP6s. The representative trial shown in Figure 4, A–C, displays how the synaptic calcium transients of three closely spaced ROIs are independent in participation in the series of stimuli and can appear to fluctuate from failures to transients of consistent amplitude (marked with dotted line). However, transients often appear to be many times larger than the minimum events, as with PSP6 at ROI3 in the example (Fig. 4A–C). Whether this apparent multiquantal synaptic transmission is the result of intrasite multivesicular release or closely spaced synapses is unclear and cannot be resolved solely by EPSCaT measurements. To resolve the independent ROIs within the large clusters of synapses sometimes observed and highlighted at the synaptic connection shown in Figure 4D, ROIs were chosen by examining responses in reverse sequence, from PSP20 to PSP1. As displayed in a montage of 12 EPSCaTs in Figure 4E, examining the independent participation of the synapses within a cluster allows for refining of the ROI set, as sites do not participate in all stimuli. Such independence of sites is visually apparent if each EPSCaT is given a different color look-up table and with all colors combined in an overlay, the color combinations can highlight the independent ROIs participating in the cluster (Fig. 4F). Selecting and refining all the ROIs using the data from all the stimuli allows separation of many of the independent ROIs within a cluster, but we do not have sufficient spatial resolution to fully separate all release sites within an ROI. Although examination of the mean ROI area (9.0 $\mu m^2 \pm 3.5$ SD, $n = 110$) over many synaptic connections finds a homogeneous distribution of ROI areas, many ROIs are twice the median, suggesting multiple synaptic sites or multiple closely spaced clusters of synaptic sites are still present (data from 10 synaptic connections). Moreover, because active zones take up an area of <1 μm^2 (Bailey and Chen 1983), there may be many clustered active zones in an individual ROI.

Large EPSCaTs represent multiquantal transmission

Even with this separation of the large clustered ROIs, many ROIs still show transients that are many multiples of the smallest transients observed at the ROI (Fig. 5A). To further examine the amplitude variance of the postsynaptic src-GCaMP6s transients at the individual ROIs (Fig. 5A) we designed a set of logic steps to automatically sort events and estimate quantal size at individual ROIs, assuming the variation is largely the result of quantal fluctuations. At each ROI, quantal size was determined by the minimum synaptic transient amplitudes and the variance of all synaptic transients at the ROI (Fig. 5B). The ROI minimum, median, and maximum event amplitudes are found, and cluster analysis used to group all events at the ROI into the minimum, median, or maximum cluster according to least difference. If the mean of the minimum cluster is >50% of the mean of the maximum cluster, all events would be averaged to find quantal size at the ROI, and such an ROI would be judged uniquantal as all events are of a consistent amplitude. At ROIs with more variation, quantal size is found from the average of the median and minimum clusters if the mean of the minimum cluster is >50% of the mean of the median cluster, if not quantal size is found from the average of the

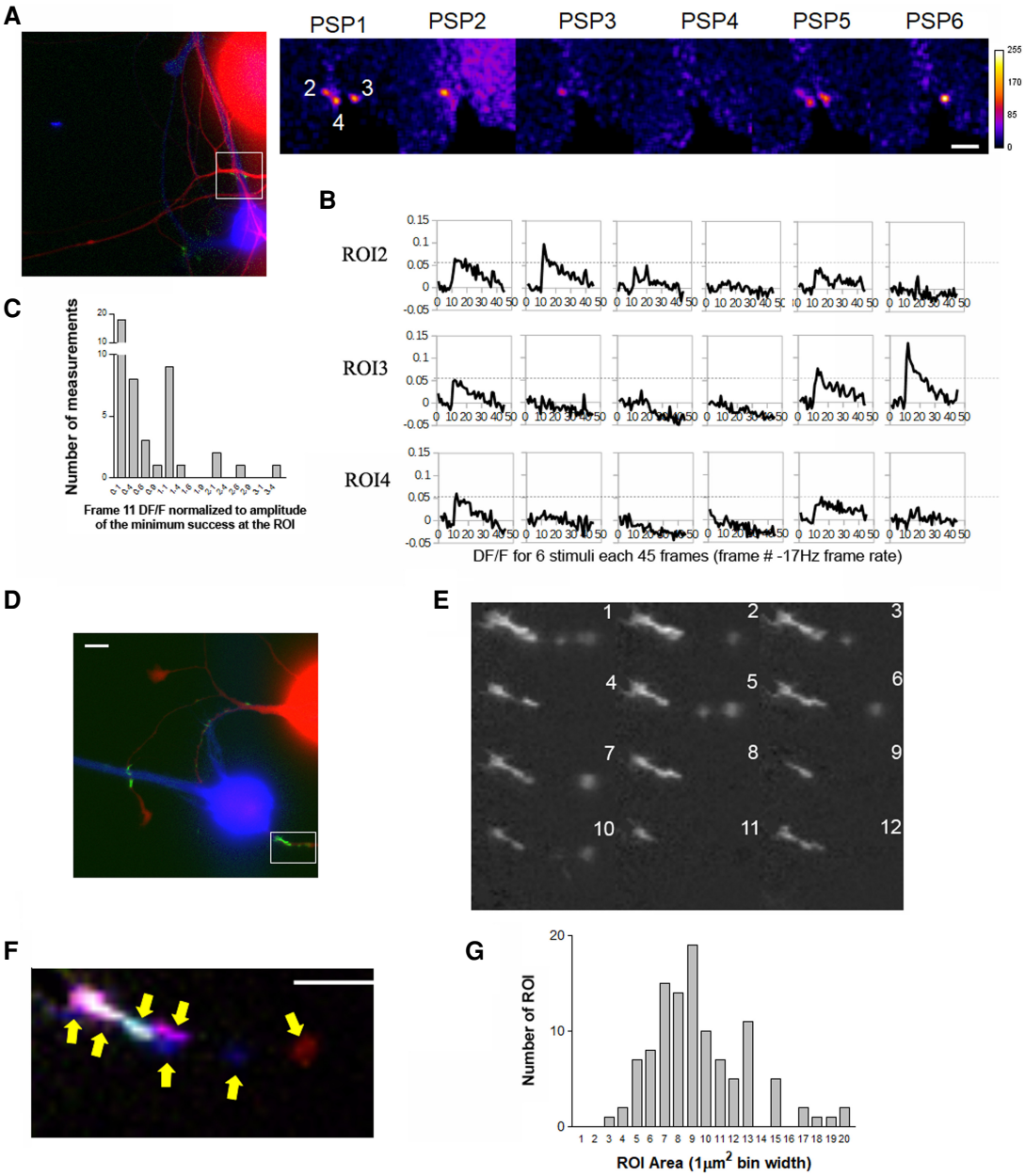

Figure 4. Quantal fluctuations and clusters of independent synapses. (*A*) *Left* image is presynaptic RFP, postsynaptic src-GCaMP6s (blue), sum of the EPSCaTs (frame 11 – frame 9) for the 20 stimuli (green), with the location of the magnified right images PSP1 to PSP6 located with the white box. The three ROIs located in this subregion show apparent quantal fluctuations with successive stimuli, visually apparent with the single stimulus EPSCaT images (frame 11 – frame 9 image subtraction generated) colored with a fire look-up table to enhance the contrast (units are arbitrary with the color palette calibration bar on the *far right*; scale bar, 10 μm). (*B*) The fluorescence intensity data from the same ROIs and stimuli shown in *A*, collected over the 45 frames converted to *DF*/*F* values. The dotted lines are for reference comparison of amplitudes within a trial. (*C*) Frequency histogram of frame 11 *DF*/*F* values for all 20 stimuli at the seven ROIs found at the synaptic connection shown in *A* (including failures of any evoked transients) normalized to the minimum observed synaptic transient at each ROI. Most events bin into the noise band and represent synaptic failures. The second peak occurs around 1 as many synaptic transients are similar in amplitude; however, events are also seen at multiples of this value. (*D*) Presynaptic RFP (red), postsynaptic src-GCaMP6s (blue), and the *DF*/*F* (green) at a representative synaptic connection with a cluster of independent synapses. (*E*) Montage of 12 successive stimuli evoked EPSCaTs at the cluster of synapses magnified from the box in *D* with the number of the stimulus in the *right top* of each image. Fluctuations in transmission at the independent sites in the cluster are apparent as sites variably participate in each stimulus. (*F*) Pseudocoloring each frame from *D* with a different color and merging them in an overlay reveals a tight cluster of independent sites marked with arrows (scale bar, 10 μm). (*G*) Frequency distribution of all ROI areas measured from 10 synaptic connections with at least five ROIs binned in 1-μm^2 bins.

minimum cluster (Fig. 5C,D). Once quantal size is estimated, a quantal content estimate can be made at each ROI for every stimulus, generating a quantal content heat map describing the synaptic connection within the field of view (Fig. 5E). From this representation of the data the success/failure probability of participation, the relative contribution of each ROI to the total quantal content, and number of ROIs participating in each stimulus can be readily derived (Fig. 5E). The sum of the quantal content

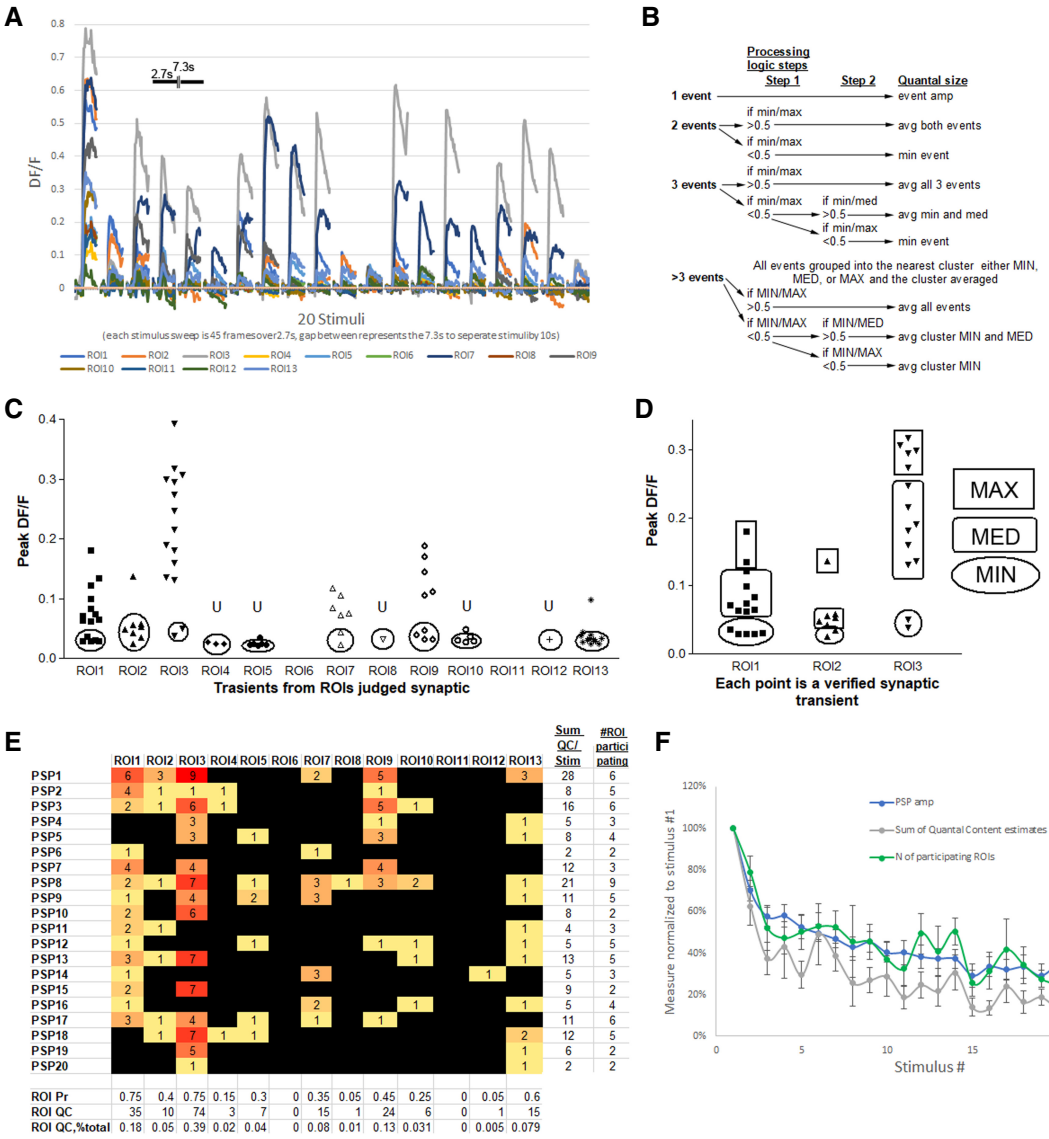

Figure 5. Deriving the parameters of synaptic transmission from the src-GCaMP6s signal at the individual ROIs. (*A*) src-GCaMP6s transients of variable amplitude from 20 successive stimuli at a representative synaptic connection with 13 ROIs identified, analyzed, and presented as in Figure 1. (*B*) Written description of the processing steps taken to determine quantal size at each ROI from the amplitude of the src-GCaMP6s transients to the 20 stimuli. Sorting and quantal size calculation was performed with Excel spreadsheets. (*C*) Peak amplitudes of transients judged synaptic at each ROI, with the group of transients averaged to determine quantal size as in *B*. Note that two ROIs fail to produce a single successful transient, because either no transient crossed the signal to noise ratio and/or no transients were judged nonsynaptic as in Figure 3. The group of transients judged uniquantal at each ROI are circled and the ROIs judged uniquantal marked with a U. (*D*) Highlighting the cluster analysis grouping outcomes for the first three ROIs from *C* shows how data with differing variances are grouped. In the example, the minimum cluster is averaged for quantal size for ROI1 and ROI3, whereas the minimum and median clusters are averaged in ROI2 based on the rules of *B*. (*E*) Following automatic determination of quantal size, ROI data can be converted to a quantal content (QC) value for each stimulus and a heat map generated to visually describe the synaptic connection as a whole over all ROIs for every stimulus. From this, the total quantal content over the 20 PSPs (ROI QC), the probability of observing a synaptic transient at the ROI (ROI Pr, as proportion of successful synaptic transients observed), and the percentage the ROIs QC contributes to total QC at the synaptic connection (ROI QC % total) can be found for each ROI. Furthermore, the summed QC and number of participating ROIs can be found for each stimulus. (*F*) Summary and comparison of the change in PSP amplitude to the sum of the quantal content estimates at all ROIs and the number of participating ROIs over the 20 stimuli recording period derived as in *E*. (Data from 10 synaptic connections.)

estimates at all ROIs and the number of ROIs participating in each stimulus reduced at similar rates over the 20 stimulus trials (normalized to the first stimulus) similar to the rate of PSP amplitude during depression (Fig. 5F). As an independent measure of quantal size, we electrophysiologically measured miniature PSPs (minis) prior to imaging action potentia–evoked transmission. If our assumption that the high variance of synaptic transient amplitude seen at some ROIs is largely the result of quantal fluctuations and if our above quantal size estimates are accurate, the amplitude variance of the src-GCaMP6s transients judged uniquantal (e.g., all the 1s in Fig. 5E) should better match the variance of mini amplitudes. Because both the minimum mini amplitude and the smallest EPSCaT at a given synaptic connection should describe the same uniquantal synaptic events, we normalized the mini data

and the EPSCaT data for each trial to the minimum observed event (smallest mini amplitude or smallest EPSCaT amplitude in that trial). When all measurements are normalized, binned, and displayed in a frequency distribution we find that the uniquantal estimates have a similar distribution and variance to the independently measured minis (Fig. 6A). The high variance observed when examining all EPSCaT amplitudes is significantly greater than both the EPSCaT's judged uniquantal and mini amplitudes, indicating that the source of most the variance at the ROIs with high transient variance is multiquantal synaptic transmission at the ROI and that our method of estimating quantal size appears accurate (Fig. 6B). Consistent with the multiquantal ROIs representing the clustering of multiple synaptic release sites, the measure of ROI release probability strongly correlated with the initial quantal content at the ROI (Pearson's $r = 0.6804$, $P < 0.0001$) (Fig. 6C).

Analysis of uniquantal ROIs does not show evidence for synaptic site silencing during homosynaptic depression

As it is likely that the multiquantal ROIs are clusters of independent synaptic release sites, we measured release probability and release site silencing at only the uniquantal ROIs to avoid averaging multiple sites that prevents differentiation of a change in the number of participating release sites from a change in release probability. Although the number of uniquantal ROIs is greater overall (58 compared with 46 multiquantal at the 10 synaptic connections), the uniquantal subset of ROIs represent a smaller fraction of the synaptic connection with much less quantal content output (~24% of the quantal content produced at the multiquantal ROIs). However, the normalized change in quantal content at the uniquantal ROIs is similar to the mulitquantal ROIs and is consistent with the kinetics of homosynaptic depression (Fig. 6D). If the uniquantal ROIs are single synapse release sites, then release probability (P_R) can be estimated and release site "silencing" can be assessed. Calculating the average P_R at each uniquantal ROI from the 20 stimuli finds an average P_R of 0.24 ± 0.04 for the uniquantal ROIs and a frequency distribution shows that most sites have a low average P_R over the 20 stimuli (Fig. 6E). Examining this same uniquantal subset of data from the 10 synaptic connections, we can measure the release probability for each stimulus and found an initial average P_R of ~0.6 at the uniquantal ROI for the first stimulus and a reduction in P_R over the course of the 20 stimuli similar to the rate of homosynaptic depression (Fig. 6F). To assess the possibility that some of the synapses "silence" leading to depression, uniquantal ROIs were examined to determine which stimulus produced the final EPSCaT over the 20 stimuli. If release site silencing leads to depression, one would expect many synapses to participate in the first few stimuli, but then drop out. This should lead to an inverse correlation between the stimulus producing the last EPSCaT at an ROI in the stimulus series and the stimulus number. Instead, there was a positive correlation (Pearson's $r = 0.5869$, $P < 0.0065$) as would be expected of release sites continuing to participate during the whole stimulus train (Fig. 6G). Although we cannot directly observe whether some putative sites within the multiquantal ROIs are "silencing" over the course of depression, the similarity in the time course and extent of homosynaptic depression observed at both multiquantal and uniquantal ROIs suggests this is unlikely and certainly not required to result in the extent of depression observed.

Most EPSCaTs are not associated with presynaptic varicosities in contact with the postsynaptic neuron

To examine whether most EPSCaTs occur apposed to presynaptic varicosities, mRFP expressed in the sensory neuron was used to blindly identify varicosities according to criteria outlined previously for sensory neuron-LFS synapses (Fig. 7A; Chen et al. 2014). Using the methods described above to select ROIs that identify the location of the synaptic elements contributing within the field of view, we find that although many varicosities contain synapses, the majority do not (Fig. 7B). Probably more importantly, most EPSCaTs are not apposed to presynaptic varicosities, but instead are localized to regions where the presynaptic neuron grows on the postsynaptic neuron without obvious thickening on either side (Fig. 7B). Thus, in the sensory neuron to motor neuron cultures used in this study, the presynaptic varicosities are not good indicators of the location of synapses defined by the EPSCaTs. As some ROIs appear to be multiquantal, we further sorted the data to examine what type of ROI tends to occur at varicosities. On average ~47% of the ROI in this data set were judged multiquantal (three or more quantal content), whereas a slightly lower percentage of ROI at varicosities were judged to be multiquantal at ~31%, indicating no trend for the occurrence of multiquantal ROI specifically at varicosities.

Postsynaptic src-GCaMP6s can be used to track synapses over multiple days

To determine whether the described methods of measuring both the strength and spatial distribution of the synapse within a particular field of view can be used to track synaptic sites over multiple days we tracked synaptic pairs over 2 d (Fig. 8). Some ROIs are clearly tracked over both days, having specific spatial localization in isolation and proximity to pre- and postsynaptic image landmarks (Fig. 8A). The quantal content heat maps generated for each day as in Figure 5 can be reorganized, so that the ROIs blindly judged to be the same between days are reorganized into a single column. Some ROIs appear to move from day to day or, alternatively, sites are lost and new sites arise (new columns) (Fig. 8B). Some sites are close to the image boundaries so that their appearance or disappearance may reflect entry or exit of the field of view, such as ROI17 and ROI20 in the example. Other ROIs are not faithfully tracked over both days, suggesting there are new synaptic sites created and old synaptic sites removed. Alternatively, the ROIs that appear may simply be dispersed from large clusters unresolvable on the previous day or conversely the loss of ROIs through clustering of multiple independent synaptic sites. Anecdotally to this, ROI19 and ROI16 that disappear on day 2 are neighboring ROI9 and ROI13, respectively, two ROIs that appear highly multiquantal and have increased quantal content on the second day of imaging suggesting the possibility of sites merging over time. Importantly, neither the presence of src-GCamP6s over multiple days nor the use of the high calcium saline for the measurement of the EPSCaTs has any toxic effect on the synapse, because PSP amplitude is constant over both days (Fig. 8C). We found no significant change in the measure of quantal size and the sum of quantal content (both measured as described in Fig. 4) nor in the number of ROIs with synaptic transients (Fig. 8C), suggesting that this technique can be used to measure changes in synaptic strength over multiple days in culture.

Discussion

Src-GCamp6S can be used to monitor synaptic locations in sensory–motor neuron cultures

A functional synapse requires presynaptic release and postsynaptic receptors. Unlike measurements such as Synapto-pHluorins or pHluorin-tagged glutamate receptors, EPSCaTs actually require a functional synapse to be measured. We are able to largely eliminate nonsynaptic calcium transients by locking our measurements to presynaptic action potentials and strict requirements for the

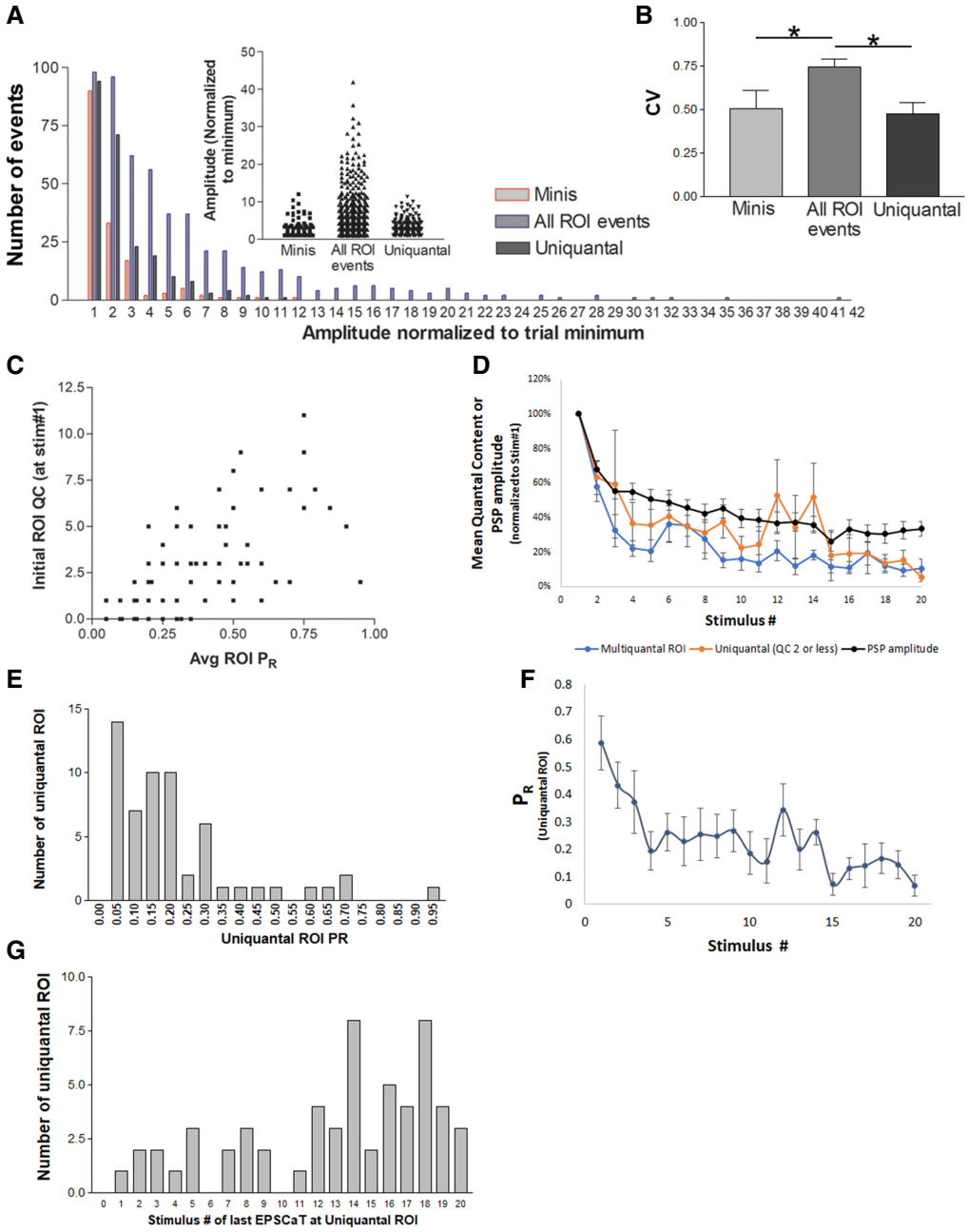

Figure 6. Estimating synaptic release site probability with the uniquantal ROI. (*A*) Comparison of the amplitude distribution of spontaneous mPSPs (minis) to the amplitude distribution of all synaptic ROI transients and to the subset of synaptic transients occurring at the uniquantal ROIs (maximum ROI quantal content of two or less) as in Figure 5. Minis were recorded prior to stimulation and only synaptic connections with >10 minis recorded were used for analysis here. Normalization of all data within a trial to the minimum value for the measure (smallest mini amplitude or smallest EPSCaT amplitude in this trial) allows comparing data between measures and from the six synaptic connections examined for variance in amplitude. (*B*) The skew in the amplitude distribution of the synaptic ROI transients judged to be uniquantal was similar to the skew of the mini PSP amplitudes, as summarized with the coefficient of variance (CV) in the normalized amplitudes. The normalized amplitude distribution of all synaptic transients measured at the ROIs was much more skewed than both the electrophysiologically measured mPSPs and the synaptic transients judged to be uniquantal with a significant increase in the CV (comparing the CV of the normalized mPSP amplitude, all synaptic ROI transients, and only the uniquantal synaptic transients with a repeated measures ANOVA). (*) $P<0.05$, $n=6$ synaptic connections. (*C*) Comparison of initial ROI quantal content measured at stimulus 1 and the average release probability of the ROI measured with all 20 stimuli. Data from 104 ROIs from 10 synaptic connections, Pearson's $r=0.6804$, $P<0.0001$. (*D*) Mean quantal content of all ROIs grouped according to maximum quantal content over the 20 stimuli series into either multiquantal (>2 QC) and uniquantal ROIs plotted along with PSP data, each measure normalized within each trial to the value at stimulus 1 ($n=9$ synaptic connections, data removed from one trial in each group for having no release at stimulus 1, PSP data from all 10 synaptic connections). (*E*) Frequency distribution of the average P_R calculated from the 20 stimuli for each of the uniquantal ROIs (max QC ≤ 2) grouped into 0.05 bins. (*F*) Average release probability of the uniquantal ROIs calculated for each stimulus over the 20 stimuli train. (*G*) Frequency distribution of which stimulus (over the 20) produced the last EPSCaT at each of the uniquantal ROIs (e.g., if the last successful transient at a uniquantal ROI was stimulus 12, then that ROI would be in bin 12). The Pearson's *r* value between the stimulus number in the sequence of homosynaptic depression and the grouped data of the number of uniquantal ROIs that may potentially "silence" (stop releasing to stimulus 20) was 0.5869 ($P=0.0065$), a significant negative correlation would be expected if this mechanism was involved in depression. Data in *E*–*G* from 58 uniquantal ROIs at 10 synaptic connections.

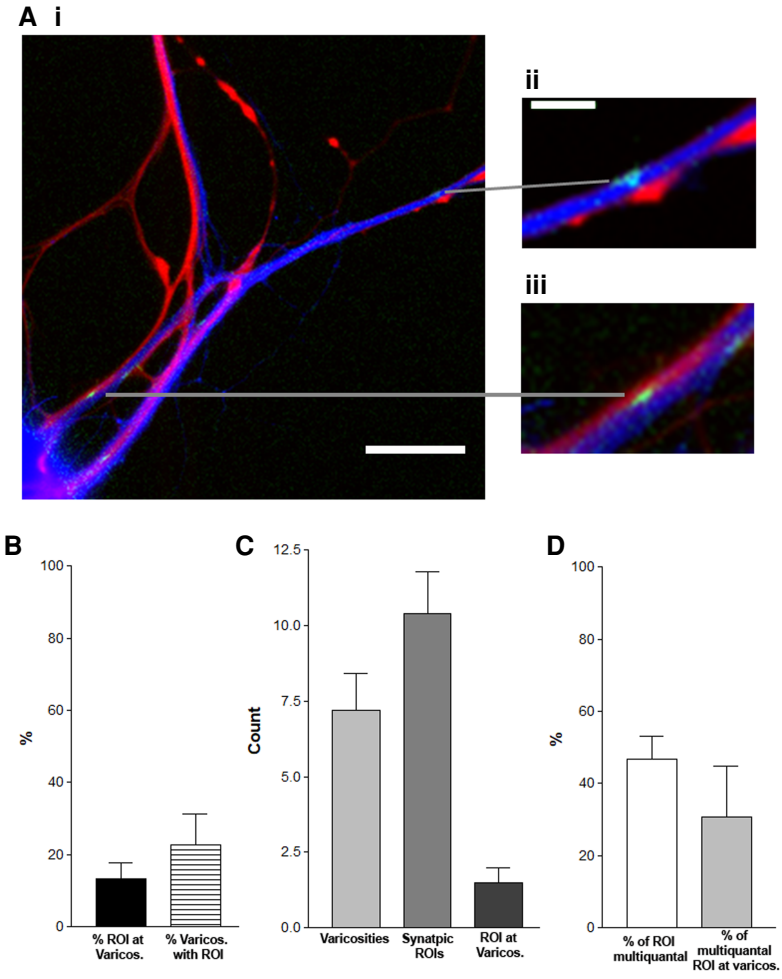

Figure 7. Synapse localization relative to presynaptic varicosities. (*A*) Representative synaptic pair with the sensory neuron expressing RFP (red), the postsynaptic neuron expressing src-GCaMP6s (blue), and the location of the synapses visualized as in Figure 1 (green). Presynaptic varicosities in contact with the postsynaptic neuron are identified by a blind judge and then compared with the location of the synaptic ROIs. An example of a synapse at a presynaptic varicosity (panel *ii*) and a synapse not at a presynaptic varicosity (panel *iii*) are shown in the *insets*. Scale bars, 40 µm (panel *i*), 10 µm (panels *ii*,*iii*). (*B*) Summary data from 10 synaptic connections, displaying the percentage of synapses (ROIs with synaptic transients) at presynaptic varicosities and the percentage of presynaptic varicosities with identified synaptic ROIs. (*C*) The average number of varicosities identified by the judges and the average number of synaptic ROIs from the data set summarized in *B*. (*D*) The percentage of all ROIs that appear multiquantal (three or more multiples of the quantal size estimate at the ROI) and the percentage of ROIs at varicosities that appear multiquantal from the data set.

timing of the rise of the EPSCaT. Moreover, because we measure 20 stimuli, we should be able to detect most synaptic release sites with a release probability of >0.05. The similar variance of uniquantal EPSCaTs and miniature PSPs suggests that the large EPSCaT fluctuations at some ROIs are multiquantal fluctuations and that individual sites with expected single quantal fluctuations are measurable. The ability to measure a single quantum of release is an important benchmark for the technique as otherwise measurement would be biased toward multiquantal sites if uniquantal sites slip below detection.

Multiquantal ROIs

Our results show that even with the improved resolution of the membrane delimited Src-GCAMP6s, many EPSCaTs still appear to be multiquantal. Although we cannot rule out the potential contribution of intrasite multivesicular release (Kusick et al. 2020), it is likely this largely results from multiple independent synaptic release sites existing in close proximity and such arrangements would not be resolvable with the methods used here. The propensity for sites to occur in clusters that are resolvable as in Figure 4 further supports the idea that the ROIs with multiquantal EPSCaTs are a tight cluster of individual synapses, as does the proportional increase in release probability with quantal content, consistent with the summation of multiple individual release sites. It is interesting that a majority of the quantal content measured by the EPSCaTs comes from these apparent multiquantal sites. If these represent clustered synapses, it will be interesting in the future to learn why synapses are clustered together in one small region of the possible contacts between the sensory and motor neuron. We did not observe any obvious way of predetermining where this was in the synaptic arbor.

It is possible that increasing spatial resolution of the imaging could partially resolve whether these are clustered synapses or sites of multivesicular release. One factor limiting spatial resolution is the wide field camera. In contrast, studies with total internal reflection fluorescence (TIRF) microscopy (Pahlavan and Morad 2017) or line scan confocal microscopy (Kong et al. 2013; Shang et al. 2014) have resolved calcium signals to <1 µM. However, these techniques would not allow us to scan the broad array of synaptic release sites in these cultures. Another limitation is the timing of imaging integration (25 msec) and the slow response of GCaMP6s (150 msec), both of which greatly exceed the time to peak of the postsynaptic current in *Aplysia* neurons (~8 msec) (Phares and Byrne 2005). With development of new calcium sensors, there is hope for increased spatial resolution in the future. Another factor limiting resolution is the lack of natural barriers to calcium diffusion. For example, spines in mammalian neurons allow for higher-resolution imaging due to the narrow spine neck and endogenous buffers decreasing calcium diffusion to neighboring spines (Metzbower et al. 2019).

Quantal resolution of synaptic sites allows examination of models of synaptic depression

Previous imaging studies of *Aplysia* synaptic connections have failed to demonstrate quantal resolution and therefore may have missed individual release sites in isolation, a strong possibility considering the tendency for release sites to cluster (Kim et al. 2003; Malkinson and Spira 2010; Malkinson and Spira 2013). If synaptic sites in clusters have similar transmission characteristics to synaptic sites in isolation, examining just the putative individual synaptic release sites in isolation (uniquantal sites) allows for a measure of single release site release probability (P_R). Our estimates of the P_R

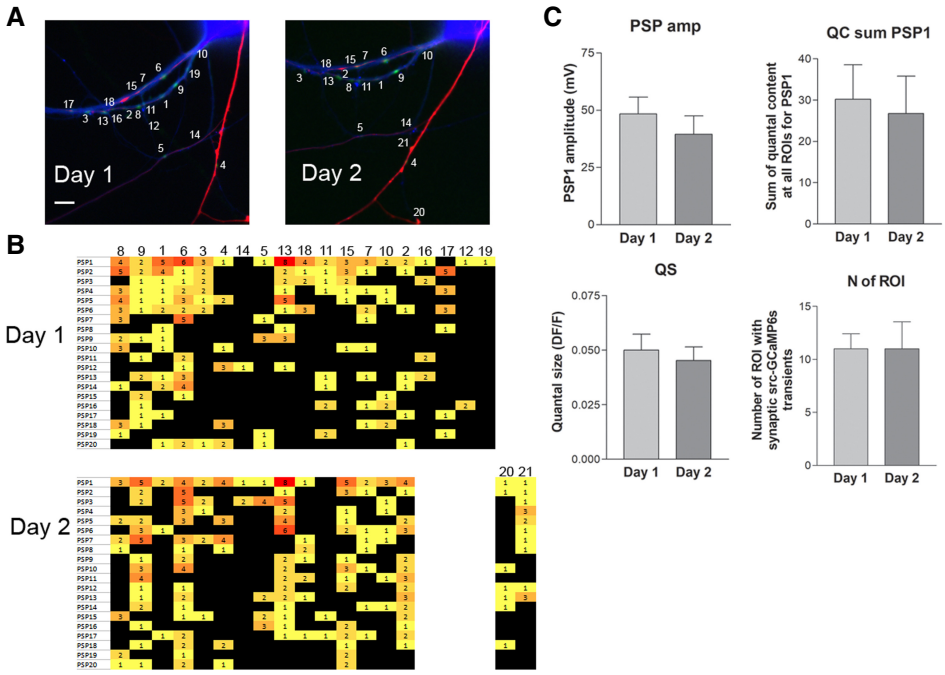

Figure 8. Tracking synapses over multiple days. (*A*) Presynaptic RFP (red), postsynaptic src-GCaMP6*s* (blue), and the sum of all the single stimulus images (each generated with frame 11 – frame 9 as in Fig. 1D) compressed into a single image marking the location of the synapses (green). ROIs highlighted are selected as described above, and a blind judge categorizes each ROI on subsequent days as either an ROI identity from a preceding day, a new ROI, an ROI that has disappeared, or an ROI that may have appeared or disappeared from the field of view. This judges table is then used to track the ROIs over multiple days. Some ROIs such as 17 and 20 may have left or entered the field of view, respectively, whereas ROIs like 12, 16, and 19 were not observed on the second day and others like 21 appear on the second day. (*B*) The quantal content heat maps generated as described in Figure 5, reorganized with the blind judges table to place ROIs judged to be the same on multiple days in the same column. Data from the same synaptic connection imaged in *A*. (*C*) Summary data from five synaptic connections followed over 2 d with at least five ROI. Mean data for the amplitude of PSP1 (in millivolts), the average sum of quantal content for PSP1 and the average quantal size both measured as described in Figure 4, and the number of ROIs with synaptic transients. Paired *t*-tests find no significant difference between any of the measures on day 1 and day 2, $P > 0.05$, $n = 5$.

at only these uniquantal sites found an average P_R of ~0.6 for the first stimulus that reduced with subsequent stimuli consistent with a reduction in P_R underlying homosynaptic depression. Some previous studies have presented evidence that release probability does not change with homosynaptic depression (Royer et al. 2000; Gover et al. 2002). The most direct measure of this was the electrophysiological measurement of synaptic variance during mid and late homosynaptic depression that was found to be stable indicating no change in release probability (Royer et al. 2000). However, the most substantial depression occurs during the first few stimuli, and more importantly, synaptic variance only has a linear relationship with release probability at low P_R values (Clements 2003; Silver 2003). Our observation that P_R reduces over the course of homosynaptic depression invalidates the assumptions required for estimating the parameters of synaptic transmission from variance-mean estimates.

Measuring the average P_R from all the uniquantal sites for each of the 20 stimuli allows for an estimate of the change in P_R for the synaptic connection over the course of homosynaptic depression, assuming these sites are indeed single synapse release sites. In support of the assumption that the uniquantal ROIs are indeed single synaptic sites are the apparent quantal fluctuations observed, the similarity in variance to minis, and the similar average release probability of these sites over the 20 stimuli. We found a reduction in P_R consistent with a decrease in release probability underlying homosynaptic depression. Although this is similar to the conclusion reached by a previous study also using EPSCaTs (Malkinson and Spira 2013), this previous study did not provide evidence for quantal resolution and thus could not differentiate between a change in the average release probability and the number of sites that can release. Previous studies suggested that homosynaptic depression occurs when a subset of synapses "silence," or stop releasing, during the low-frequency stimulus train (Royer et al. 2000; Gover et al. 2002). Examining our subset of uniquantal sites did not reveal a tendency for sites to silence, instead only ~5% of these sites ceased to release after the first two stimuli, far too few to account for the dramatic reduction in transmitter release during this period of depression. Neither a reduction in the ready releasable pool of synaptic vesicles (Gingrich and Byrne 1985; Bailey and Chen 1988; Angers et al. 2002; Zhao and Klein 2002) nor a reduction in presynaptic calcium influx through voltage-gated calcium channels (Armitage and Siegelbaum 1998; Malkinson and Spira 2013) can fully account for the decrease in synaptic transmission seen during homosynaptic depression. Our data, along with these previous results, suggest that a reduction in release probability underlies homosynaptic depression, and that this reduction occurs through a mechanism downstream from presynaptic calcium entry and at least partially upstream of RRP maintenance.

Relationship between varicosities and synaptic sites

We find that only ~25% of the presynaptic varicosities have EPSCaTs apposed to them. These numbers are smaller than those found with EPSCaTs measured with a calcium dye (56%) (Malkinson and Spira 2010), the number of presynaptic varicosities that have active release sites as measured with Synapto-pHluorin (30%) (Kim et al. 2003), and the number of presynaptic varicosities in the animal that have active zones (40%) (Bailey and Chen 1983). For Synapto-pHluorin and presynaptic varicosities in the animal,

stimulation that leads to long-term facilitation/sensitization increases the percentage of presynaptic varicosities with release sites and with active zones (Bailey and Chen 1983; Kim et al. 2003). We have not yet examined our results after inducing plasticity, and thus it is likely that the percentage of varicosities that have synapses may increase under these conditions. Other differences between these studies and ours that could account for the differences are criteria for defining presynaptic varicosities (we used blind measurements using a defined criteria [10 μm^2 and an oval shape] [Chen et al. 2014], whereas most studies do not define the criteria used and assignment was not done blindly), the type of preparation (these preparations used L7, and the present study used LFS neurons), or other unknown culture conditions. The more striking finding is the large number of EPSCaTs that occur at sites not adjoining presynaptic varicosities (>80% in our preparation). This is approximately double the number previously measured with EPSCaTs in L7 neurons. However, without confirmation of quantal resolution in this study, there remains doubt that all the synapses within the field of view were measured (Malkinson and Spira 2010). This difference, similar to above, could be due to differences between L7 and LFS neurons, differences in the details of the culture conditions, differences in the definition of a varicosity, and the focus on varicosity rich regions in the previous study. Earlier studies in L7 with EM to examine where active zones were located in cultures (Glanzman et al. 1989) or using Synapto-pHluorins to define release sites (Kim et al. 2003) only focused on synaptic varicosities and thus did not calculate the percentage of active zones or vesicular release sites that were not apposed to varicosities.

Another quality found with this resolution of the synapse was the propensity for the underlying elements to cluster together, further reducing the spatial location of synaptic activity to very small areas within the pre- and postsynaptic contact. Our results strongly demonstrate that, in some circumstances, synapses in *Aplysia* sensory neuron to motor neuron cultures are not always primarily located at presynaptic varicosities. Thus, the use of varicosities as a surrogate for synaptic sites could be misleading.

The use of EPSCaTs to follow synapses over time

The ability to follow individual synaptic elements over time will allow us to determine what molecular elements may determine the stability of individual synapses and if certain synapses are particularly sensitive to memory-disrupting agents such as inhibitors of persistently active kinases (Chen et al. 2014). The stability of synaptic efficacy over 2 d indicates that the sensor and the measurements do not affect the synapse, whereas the stability of the quantal size estimate demonstrates that the src-GCaMP6s synaptic subpopulation is consistent over 2 d, allowing for the faithful detection of synaptic transmission. A variety of issues complicate the interpretation of the tracking of the synapses over multiple days. Some sites appear to move and thus can enter or leave a field of view. However, the average of leaving and entering should even out for measuring the total number of sites. The apparent clustering of individual release sites is problematic for the calculation of release site P_R and it also complicates measurement of the number of sites, as presumably release sites may enter or leave the clusters. If new synapses appear within a previous multiquantal ROI, this will change the quantal content of the ROI, but it will not be possible to differentiate an increase in quantal amplitude of a cluster (i.e., through an increase in AMPA receptor number), with an increase in the number of synapses in the cluster. Similarly, new synapses appearing in a multiquantal ROI will likely increase the measured P_R at that ROI, but cannot be distinguished from a change in P_R without addition of new synapses. However, none of these issues will affect our ability to detect the addition of uniquantal ROIs and changes in uniquantal P_R and amplitude. Thus, with the assumption, similar to what we observed here for synaptic depression, that multiquantal ROIs and uniquantal ROIs are regulated in a similar manner, this technique may be able to answer the still-open question of how long-term changes in synaptic strength are maintained in this system by focusing on changes at uniquantal ROIs.

Materials and Methods

Src-GCaMP6s generation

The generation of pNEXp-APsrc-gCAMP6s (Src-GCaMP6s) with the first 34 amino acids of *Aplysia* Src (NP_001191639.1) inserted in front of GCaMP6s was previously described (Farah et al. 2019). The first 34 amino acids of *Aplysia* Src contain conserved myristoylation and palmitylation sites that lead to membrane insertion.

Cell culture

Aplysia were obtained from the National Resource for Aplysia at the University of Miami and maintained in holding tanks until use. *Aplysia* ganglia were digested in dispase II, and pleural sensory neurons were paired in isolation with LFS motor neurons in an isotonic L-15 based culture media containing 30% hemolymph and supplemented with L-glutamine in glass-bottomed culture dishes and left for 2 d. On day 3 in culture, the nuclei of the neurons were injected with pNEX3 expression plasmids (Kaang 1996) containing RFP (presynaptic neuron) and src-GCaMP6s (postsynaptic neuron). An additional 24 h was allowed for plasmid expression before measuring synaptic transmission. For multiday recordings, a portion of the culture media is retained so that when the day 1 recordings are finished the recording saline can be immediately replaced with fresh culture media (freshly supplemented with L-glutamine).

Electrophysiology

On day 4, cell pairs expressing RFP presynaptically and src-GCaMP6s postsynaptically are examined in a high calcium recording saline (460 mM NaCl, 55 mM $CaCl_2$, 10 mM $MgCl_2$, 10 mM KCl, 10 mM HEPES, 10 mM D-glucose at pH 7.6). Sharp electrodes (~15 MO, back-filled with saturated potassium acetate) were used to control and hold membrane potential at −80 mV and generate action potentials with an Axoclamp 900 and Digidata 1440 (Molecular Devices). Spontaneous miniature "mini" PSPs were measured for a couple of minutes prior to evoked presynaptic stimuli. Minis were identified and were measured with Clampfit (Molecular Devices) template event detection, using a template prepared previously from >100 minis at *Aplysia* pleural sensory neuron to LFS motor neuron synapses. Presynaptic action potentials are generated with a superthreshold depolarizing pulse 10 msec in duration 0.56 sec into to the acquisition period initiated with activation of the imaging software. PSP amplitude was measured with Clampfit.

Fluorescence imaging

Cell pairs were imaged with a Zeiss Axio Observer D1, with a EC Plan Neofluar 1.3 NA 40× oil coupled lens and a QuantEM: 512SC EM-CCD camera (Photometrics). Fluorescence excitation and emission achieved with an X-cite Expo arc, through Zeiss RFP 20 and Zeiss GFP 38 filter cubes. For each stimulus, 45 frames are acquired at 16.7 frames/sec, with a constant 25-msec exposure time at all trials, adjusting for baseline intensity differences between trials with camera gain. Rapid image acquisition was achieved with a Zeiss SVB-1 microscope signal distribution box and Axiovision 4.8 software using the fast acquisition application (Zeiss). Initiation of the Axiovision image acquisition electronically triggers the electrophysiological recording and therefore the stimulus to ensure that the presynaptic action potential is evoked at the same time in each 45-frame acquisition period, usually during frame 10 (slight differences in the membrane properties between the different sensory neurons varies the precise timing of

action potential generation relative to the image acquisition between the different synaptic connections examined).

ROI selection

All image analysis was done with ImageJ (Schneider et al. 2012) and Excel or Calc spreadsheets (Microsoft, LibreOffice). Subtraction of frame 9 from frame 11 generates an image of the src-GCaMP6s transients occurring during the stimulus. This image is then smoothed (each pixel converted to average of its 3 × 3 neighborhood) to aid in generation of clean ROI borders, and ROIs selected with the wand tool to draw an ROI boundary that best fits the shape of the transient. Once an ROI has been selected, the time course of the fluorescence signal at the ROI is examined over the 45 frames to ensure that it did not initiate before frame 10 and that the kinetics are consistent with a synaptic transient (i.e., rapid rise to a clear peak and slower decay than rise). Once an ROI is selected at a stimulus it cannot be removed with selection of further ROIs for subsequent stimuli within a trial. ROIs chosen in a previously analyzed stimulus within a trial can only be further divided into a cluster of smaller ROIs with analysis of subsequent stimuli. To aid in separation of closely spaced ROIs, ROI selection is done from PSP20 (stimulus 20) backward to PSP1, as the first stimulus has the most amount of synaptic activity, blurring closely spaced ROI boundaries. Following creation of the full ROI set for a particular synaptic connection, fluorescence intensity is measured for all stimuli using this full ROI set.

Varicosity measurement

A blind observer was given images of the field of view with mRFP filling the sensory neuron and Src-gCAMP6s filling the motor neuron. Using the criteria defined previously for LFS neurons (Chen et al. 2014) of a minimum size of 10 μm^2 and an oval shape, mRFP-filled varicosities were identified. After varicosities were defined, they were aligned with the location of EPSCaTs and a determination made as to whether the varicosity was associated with the EPSCaTs.

Fluorescence intensity measurements

Fluorescence intensity measurements for all 20 stimuli at the full ROI set for a particular synaptic connection were analyzed in Excel, in which data were first normalized using the average fluorescence intensity of frames 1–9 at each ROI and for each stimulus to give F_0. All fluorescence intensity measurements were normalized as $(F(t)–F_0)/F_0$ or DF/F, for the $t = 45$ frames. The standard deviation of frames 1–9 is used to measure the noise band before the stimulus for each ROI and every stimulus to define a signal detection limit. For a src-GCaMP6s transient to be considered a synaptic signal and further examined with quantal analysis, the DF/F at frame 11 needs to be greater than three times the standard deviation of frames 1–9. Visualization of this transient is achieved by subtracting the intensity values for each pixel in the image of frame 9 from the image of frame 11, creating an image of the src-GCaMP6s transient during the stimulus (see Fig. 1B). To visualize the transients at all the synapses participating over the 20 stimuli, the pixel intensity values of each of the above generated single stimulus transients are summed over all 20 stimuli to produce a single summated image of all the synaptic transients in a trial (see Fig. 1C). Note that in this image the intensity of an ROI is proportional to the quantal content at the site, and nonsynaptic calcium events that occur during any of the stimuli can enter this image (see below). Not all ROI chosen have a synaptic transient either because no transient is 3×SD 1–9, or all transients are eliminated because of nonsynaptic calcium events. Thus, in the manuscript we distinguish between the "ROI set" and the "ROI set of synaptic transients."

If the frame preceding the stimulus has a fluorescent intensity change greater than the noise band for a stimulus at an ROI (DF/F frame 9 > 3×SD frame 1–8), the transient is considered not from calcium entering synaptic glutamate receptors (nonsynaptic) as it initiated prior to the stimulus and is thus removed from subsequent analysis. So that the excitatory postsynaptic calcium transient (EPSCaT) for a specific stimulus is measured from the sum of DF/F changes at all ROIs except those with a nonsynaptic transient preceding the stimulus as above. Examination of 18 synaptic connections with at least five ROIs finds the rate of these nonsynaptic calcium events can vary from trial to trial and from recording period to recording period ranging from none observed, up to ∼4%, averaging 0.9% ± 0.2%. Similarly, it can be estimated that a similar percentage of nonsynaptic events initiate at frame 10 or 11 and thus coincidentally with the synaptic transients. Thus, about ∼1% of the transients at ROIs judged as synaptic events are likely false positive nonsynaptic transients. Such events can enter the images generated for the src-GCaMP6s transients as nonsynaptic events, so not all fluorescence observed in these calculated images represents synaptic transients.

Quantal analysis

Quantal size estimates were made at each ROI using the variance in the successful synaptic transients at each specific ROI. The estimates were made automatically with Excel spreadsheets using a cluster analysis. At each ROI, the minimum, median, and maximum src-GCaMP6s synaptic transients are found. All events are then put in a cluster according to proximity to either the minimum, median, or maximum. The similarity of the cluster means is used to calculate quantal size: If the mean of the minimum cluster is >50% of the mean of the maximum, all events are considered uniquantal and averaged. If not, but the mean of the minimum is >50% of the mean of the median, then all events in the minimum and median clusters are averaged for quantal size. Otherwise, only the mean of the minimum events is used to estimate quantal size. The 50% threshold used to find similarity between clusters was chosen as quantal increments would lead to transients twice the amplitude of the minimum with two quanta released; thus, the minimum would be half or less with multiquantal synaptic transmission at an ROI.

Statistical analysis

Statistical analyses were performed in GraphPad Prism and Microsoft Excel. The larger data set for these experiments is from 13 synaptic pairs with at least five ROIs with at least one transient judged to be synaptic; one trial excluded as an ROI did not have a failure (a feature excluding quantal analysis) and two trials were excluded for a lack of correlation between PSP amplitude and the EPSCaT amplitude (as presented in Fig. 1, both of which appear to lose correlation because of large amounts of nonsynaptic calcium transients). Five trials were examined on two consecutive days. In some cases (e.g., data on nonsynaptic transients), we use data from both days resulting in 18 synaptic pairs examined. Correlation of PSP amplitude to EPSCaT transient intensity was measured with a Pearson's r calculation in Excel and a test statistic generated with the data set compared with a Student's t-distribution to generate a P-value.

All values are means ± standard error of the mean unless specifically stated otherwise.

Acknowledgments

This work was supported by Canadian Institutes of Health Research (CIHR) grant 340328 and a Natural Sciences and Engineering Research Council of Canada (NSERC) Discovery grant to W.S.S. W.S.S. is a James McGill Professor.

References

Akbergenova Y, Cunningham KL, Zhang YV, Weiss S, Littleton JT. 2018. Characterization of developmental and molecular factors underlying release heterogeneity at *Drosophila* synapses. *Elife* **7:** e38268. doi:10.7554/eLife.38268

Angers A, Fioravante D, Chin J, Cleary LJ, Bean AJ, Byrne JH. 2002. Serotonin stimulates phosphorylation of *Aplysia* synapsin and alters its subcellular distribution in sensory neurons. *J Neurosci* **22:** 5412–5422. doi:10.1523/JNEUROSCI.22-13-05412.2002

Armitage BA, Siegelbaum SA. 1998. Presynaptic induction and expression of homosynaptic depression at *Aplysia* sensorimotor neuron synapses. *J Neurosci* **18:** 8770–8779. doi:10.1523/JNEUROSCI.18-21-08770.1998
Bailey CH, Chen M. 1983. Morphological basis of long-term habituation and sensitization in *Aplysia*. *Science* **220:** 91–93. doi:10.1126/science.6828885
Bailey CH, Chen M. 1988. Long-term memory in *Aplysia* modulates the total number of varicosities of single identified sensory neurons. *Proc Natl Acad Sci* **85:** 2373–2377. doi:10.1073/pnas.85.7.2373
Bailey CH, Kandel ER, Harris KM. 2015. Structural components of synaptic plasticity and memory consolidation. *Cold Spring Harb Perspect Biol* **7:** a021758. doi:10.1101/cshperspect.a021758
Cai D, Pearce K, Chen S, Glanzman DL. 2011. Protein kinase M maintains long-term sensitization and long-term facilitation in *Aplysia*. *J Neurosci* **31:** 6421–6431. doi:10.1523/JNEUROSCI.4744-10.2011
Casadio A, Martin KC, Giustetto M, Zhu H, Chen M, Bartsch D, Bailey CH, Kandel ER. 1999. A transient, neuron-wide form of CREB-mediated long-term facilitation can be stabilized at specific synapses by local protein synthesis. *Cell* **99:** 221–237. doi:10.1016/S0092-8674(00)81653-0
Chen S, Cai D, Pearce K, Sun PY, Roberts AC, Glanzman DL. 2014. Reinstatement of long-term memory following erasure of its behavioral and synaptic expression in *Aplysia*. *Elife* **3:** e03896. doi:10.7554/eLife.03896
Choi JH, Sim SE, Kim JI, Choi DI, Oh J, Ye S, Lee J, Kim T, Ko HG, Lim CS, et al. 2018. Interregional synaptic maps among engram cells underlie memory formation. *Science* **360:** 430–435. doi:10.1126/science.aas9204
Clements JD. 2003. Variance-mean analysis: a simple and reliable approach for investigating synaptic transmission and modulation. *J Neurosci Methods* **130:** 115–125. doi:10.1016/j.jneumeth.2003.09.019
Farah CA, Dunn TW, Hastings MH, Ferguson L, Gao C, Gong K, Sossin WS. 2019. A role for Numb in protein kinase M (PKM)-mediated increase in surface AMPA receptors during facilitation in *Aplysia*. *J Neurochem* **150:** 366–384. doi:10.1111/jnc.14807
Gingrich KJ, Byrne JH. 1985. Simulation of synaptic depression, posttetanic potentiation, and presynaptic facilitation of synaptic potentials from sensory neurons mediating gill-withdrawal reflex in *Aplysia*. *J Neurophysiol* **53:** 652–669. doi:10.1152/jn.1985.53.3.652
Glanzman DL, Kandel ER, Schacher S. 1989. Identified target motor neuron regulates neurite outgrowth and synapse formation of *Aplysia* sensory neurons in vitro. *Neuron* **3:** 441–450. doi:10.1016/0896-6273(89)90203-1
Glanzman DL, Kandel ER, Schacher S. 1990. Target-dependent structural changes accompanying long-term synaptic facilitation in *Aplysia* neurons. *Science* **249:** 799–802. doi:10.1126/science.2389145
Gover TD, Abrams TW. 2009. Insights into a molecular switch that gates sensory neuron synapses during habituation in *Aplysia*. *Neurobiol Learn Mem* **92:** 155–165. doi:10.1016/j.nlm.2009.03.006
Gover TD, Jiang XY, Abrams TW. 2002. Persistent, exocytosis-independent silencing of release sites underlies homosynaptic depression at sensory synapses in *Aplysia*. *J Neurosci* **22:** 1942–1955. doi:10.1523/JNEUROSCI.22-05-01942.2002
Greer JB, Khuri S, Fieber LA. 2017. Phylogenetic analysis of ionotropic L-glutamate receptor genes in the Bilateria, with special notes on *Aplysia californica*. *BMC Evol Biol* **17:** 11. doi:10.1186/s12862-016-0871-1
Hu J, Schacher S. 2015. Persistent associative plasticity at an identified synapse underlying classical conditioning becomes labile with short-term homosynaptic activation. *J Neurosci* **35:** 16159–16170. doi:10.1523/JNEUROSCI.2034-15.2015
Hu J, Adler K, Farah CA, Hastings MH, Sossin WS, Schacher S. 2017a. Cell-specific PKM isoforms contribute to the maintenance of different forms of persistent long-term synaptic plasticity. *J Neurosci* **37:** 2746–2763. doi:10.1523/JNEUROSCI.2805-16.2017
Hu J, Ferguson L, Adler K, Farah CA, Hastings MH, Sossin WS, Schacher S. 2017b. Selective erasure of distinct forms of long-term synaptic plasticity underlying different forms of memory in the same postsynaptic neuron. *Curr Biol* **27:** 1888–1899 e1884. doi:10.1016/j.cub.2017.05.081
Kaang BK. 1996. Parameters influencing ectopic gene expression in *Aplysia* neurons. *Neurosci Lett* **221:** 29–32. doi:10.1016/S0304-3940(96)13279-1
Kandel ER. 2001. The molecular biology of memory storage: a dialogue between genes and synapses. *Science* **294:** 1030–1038. doi:10.1126/science.1067020
Kim WB, Cho JH. 2020. Encoding of contextual fear memory in hippocampal-amygdala circuit. *Nat Commun* **11:** 1382. doi:10.1038/s41467-020-15121-2
Kim JH, Udo H, Li HL, Youn TY, Chen M, Kandel ER, Bailey CH. 2003. Presynaptic activation of silent synapses and growth of new synapses contribute to intermediate and long-term facilitation in *Aplysia*. *Neuron* **40:** 151–165. doi:10.1016/S0896-6273(03)00595-6
Kong CH, Laver DR, Cannell MB. 2013. Extraction of sub-microscopic Ca fluxes from blurred and noisy fluorescent indicator images with a detailed model fitting approach. *PLoS Comput Biol* **9:** e1002931. doi:10.1371/journal.pcbi.1002931
Kusick GF, Chin M, Raychaudhuri S, Lippmann K, Adula KP, Hujber EJ, Vu T, Davis MW, Jorgensen EM, Watanabe S. 2020. Synaptic vesicles transiently dock to refill release sites. *Nat Neurosci* **23:** 1329–1338. doi:10.1038/s41593-020-00716-1
Lee SH, Kwak C, Shim J, Kim JE, Choi SL, Kim HF, Jang DJ, Lee JA, Lee K, Lee CH, et al. 2012. A cellular model of memory reconsolidation involves reactivation-induced destabilization and restabilization at the sensorimotor synapse in *Aplysia*. *Proc Natl Acad Sci* **109:** 14200–14205. doi:10.1073/pnas.1211997109
Li Y, Dharkar P, Han TH, Serpe M, Lee CH, Mayer ML. 2016. Novel functional properties of *Drosophila* CNS glutamate receptors. *Neuron* **92:** 1036–1048. doi:10.1016/j.neuron.2016.10.058
Malkinson G, Spira ME. 2010. Imaging and analysis of evoked excitatory-postsynaptic-calcium-transients by individual presynaptic-boutons of cultured *Aplysia* sensorimotor synapse. *Cell Calcium* **47:** 315–325. doi:10.1016/j.ceca.2009.12.015
Malkinson G, Spira ME. 2013. Release properties of individual presynaptic boutons expressed during homosynaptic depression and heterosynaptic facilitation of the *Aplysia* sensorimotor synapse. *Front Cell Neurosci* **7:** 165. doi:10.3389/fncel.2013.00165
Metzbower SR, Joo Y, Benavides DR, Blanpied TA. 2019. Properties of individual hippocampal synapses influencing NMDA-receptor activation by spontaneous neurotransmission. *eNeuro* **6:** ENEURO.0419-18.2019. doi:10.1523/ENEURO.0419-18.2019
Nagakura I, Ormond J, Sossin WS. 2008. Mechanisms regulating ApTrkl, a Trk-like receptor in *Aplysia* sensory neurons. *J Neurosci Res* **86:** 2876–2883. doi:10.1002/jnr.21741
Nakai J, Ohkura M, Imoto K. 2001. A high signal-to-noise Ca^{2+} probe composed of a single green fluorescent protein. *Nat Biotechnol* **19:** 137–141. doi:10.1038/84397
Pahlavan S, Morad M. 2017. Total internal reflectance fluorescence imaging of genetically engineered ryanodine receptor-targeted Ca^{2+} probes in rat ventricular myocytes. *Cell Calcium* **66:** 98–110. doi:10.1016/j.ceca.2017.07.003
Paredes RM, Etzler JC, Watts LT, Zheng W, Lechleiter JD. 2008. Chemical calcium indicators. *Methods* **46:** 143–151. doi:10.1016/j.ymeth.2008.09.025
Phares GA, Byrne JH. 2005. Analysis of 5-HT-induced short-term facilitation at *Aplysia* sensorimotor synapse during bursts: increased synaptic gain that does not require ERK activation. *J Neurophysiol* **94:** 871–877. doi:10.1152/jn.01261.2004
Royer S, Coulson RL, Klein M. 2000. Switching off and on of synaptic sites at *Aplysia* sensorimotor synapses. *J Neurosci* **20:** 626–638. doi:10.1523/JNEUROSCI.20-02-00626.2000
Schneider CA, Rasband WS, Eliceiri KW. 2012. NIH Image to ImageJ: 25 years of image analysis. *Nat Methods* **9:** 671–675. doi:10.1038/nmeth.2089
Shang W, Lu F, Sun T, Xu J, Li LL, Wang Y, Wang G, Chen L, Wang X, Cannell MB, et al. 2014. Imaging Ca^{2+} nanosparks in heart with a new targeted biosensor. *Circ Res* **114:** 412–420. doi:10.1161/CIRCRESAHA.114.302938
Shigetomi E, Kracun S, Sofroniew MV, Khakh BS. 2010. A genetically targeted optical sensor to monitor calcium signals in astrocyte processes. *Nat Neurosci* **13:** 759–766. doi:10.1038/nn.2557
Silver RA. 2003. Estimation of nonuniform quantal parameters with multiple-probability fluctuation analysis: theory, application and limitations. *J Neurosci Methods* **130:** 127–141. doi:10.1016/j.jneumeth.2003.09.030
Sossin WS. 2008. Defining memories by their distinct molecular traces. *Trends Neurosci* **31:** 170–175. doi:10.1016/j.tins.2008.01.001
Sossin WS. 2018. Memory synapses are defined by distinct molecular complexes: a proposal. *Front Synaptic Neurosci* **10:** 5. doi:10.3389/fnsyn.2018.00005
Sun ZY, Schacher S. 1998. Binding of serotonin to receptors at multiple sites is required for structural plasticity accompanying long-term facilitation of *Aplysia* sensorimotor synapses. *J Neurosci* **18:** 3991–4000. doi:10.1523/JNEUROSCI.18-11-03991.1998
Wainwright ML, Zhang H, Byrne JH, Cleary LJ. 2002. Localized neuronal outgrowth induced by long-term sensitization training in *Aplysia*. *J Neurosci* **22:** 4132–4141. doi:10.1523/JNEUROSCI.22-10-04132.2002
Zhao Y, Klein M. 2002. Modulation of the readily releasable pool of transmitter and of excitation-secretion coupling by activity and by serotonin at *Aplysia* sensorimotor synapses in culture. *J Neurosci* **22:** 10671–10679. doi:10.1523/JNEUROSCI.22-24-10671.2002

Received March 10, 2021; accepted in revised form June 26, 2021.